Materials Today Communications 51 (2026) 114717

Contents lists available at ScienceDirect

Materials Today Communications

journal homepage: www.elsevier.com/locate/mtcomm

Eco-inspired synthesis of silver nanoparticles from *Prunus avium* stems: Mechanistic insights into multifunctional biomedical activities

Hamideh Dehghan [a,b,1], Pouria Mohammadparast-Tabas [c,d,1], Alireza Ghasempour [a,e], Yasaman Soleimanmanesh [f], Marzieh Jafari Bidhendi [g], Fatemeh Sadat Nabavi sales [c], Alemeh Gholami [c], Majid Zare-Bidaki [h,*], Sobhan Mortazavi-Derazkola [i,*]

[a] *Student Research Committee, Mashhad University of Medical Sciences, Mashhad, Iran*
[b] *Department of Medical Biotechnology and Nanotechnology, Faculty of Medicine, Mashhad University of Medical Sciences, Mashhad, Iran*
[c] *Student Research Committee, Birjand University of Medical Sciences, Birjand, Iran*
[d] *Department of Medical Biotechnology, School of Medicine, Birjand University of Medical Sciences, Birjand, Iran*
[e] *Immunology Research Center, Mashhad University of Medical Sciences, Mashhad, Iran*
[f] *School of Medicine, Guilan University of Medical Sciences, Rasht, Iran*
[g] *Department of Chemistry, Faculty of Science, Islamic Azad University, North Tehran Branch, Tehran, Iran*
[h] *Infectious Diseases Research Center, Birjand University of Medical Sciences, Birjand, Iran*
[i] *Medical Toxicology and Drug Abuse Research Center (MTDRC), Birjand University of Medical Sciences, Birjand, Iran*

ARTICLE INFO

Keywords:
Silver nanoparticle
Green synthesis
Antioxidant
Antibacterial
Wound healing

ABSTRACT

Silver nanoparticles (AgNPs) fabricated via green approaches have emerged as attractive candidates for multifunctional biomedical applications. In the present work, an environmentally benign method was employed to synthesize AgNPs using *Prunus avium L.* stem extract (AgNPs@*PAS*), followed by detailed physicochemical characterization with different techniques. Structural analyses verified the formation of predominantly spherical AgNPs@*PAS* with particle sizes mainly ranging from 10 to 35 nm, while FT-IR spectra confirmed the presence of phytochemical compounds acting as surface-capping agents. Biological investigations revealed broad-spectrum antibacterial properties, with the highest efficacy observed against *Escherichia coli* (MBC= 140 μg/mL), as well as considerable antifungal activity against *Candida albicans* (MIC= 17.5 μg/mL). The synthesized AgNPs@*PAS* also displayed strong antioxidant performance, achieving 93 % DPPH radical scavenging at a concentration of 140 μg/mL. Furthermore, in vivo burn wound experiments illustrated a significant enhancement in wound closure following treatment with AgNPs@*PAS*. Cytotoxicity assessment indicated notable anticancer property on the MCF-7 breast cancer cell line, with an IC_{50} value of 78.8 μg/mL. Collectively, these results suggest that AgNPs@*PAS* represent a promising multifunctional nanoplatform for biomedical applications, particularly in burn wound healing.

1. Introduction

Damage to the skin disrupts its protective barrier function, increasing susceptibility to infection and highlighting the complexity of the wound healing process [1]. On the other hand, the treatment of infected skin wounds represents a major medical challenge, as a protracted infection can lead to delayed wound healing and impaired growth of the blood vessels [2]. Given the limitations associated with current wound care strategies, there is an urgent need for innovative approaches capable of promoting efficient, sustained tissue repair and improving patients' quality of life [1,3,4].

Nanoparticles exhibit unique physicochemical characteristics (like their small size and high surface-to-volume ratio) that distinguish them from bulk materials and enable enhanced biological interactions [5]. A variety of nanoparticles have been applied in different fields. Among them, silver nanoparticles have attracted considerable attention due to their broad applicability in electronics, agriculture, packaging, pharmaceuticals, and medicine [6,7]. Numerous studies have demonstrated the therapeutic potential of AgNPs, reporting significant antibacterial, antifungal, anti-inflammatory, antioxidant, anticancer, and

* Corresponding authors.
E-mail addresses: m.zare@live.co.uk (M. Zare-Bidaki), S.mortazavi23@yahoo.com (S. Mortazavi-Derazkola).
[1] *These authors contributed equally to this work.*

https://doi.org/10.1016/j.mtcomm.2026.114717
Received 30 September 2025; Received in revised form 5 January 2026; Accepted 21 January 2026
Available online 22 January 2026

wound-healing activities [5]. Fatima et al. showed that AgNPs not only possess strong antibacterial activity but also accelerate wound healing [8], while Khorrami et al. reported that AgNPs exert potent anticancer effects by reducing the viability of breast cancer cell lines [9].

Silver nanoparticles can be fabricated using various methods [10]. Physical and chemical synthesis approaches, however, are often expensive, environmentally harmful, and may involve toxic reagents [11]. In contrast, green synthesis offers a safer, cleaner, and more cost-effective alternative, particularly for biomedical applications, as it typically utilizes plant extracts or other biological materials [10]. Notably, plant-mediated synthesis endows the resulting nanoparticles not only with the inherent properties of silver but also with the bioactive characteristics of the plant-derived phytocompounds, potentially enhancing their therapeutic performance [5]. In recent years, various biological extracts and microbial sources have been successfully utilized for the green synthesis of nanomaterials. Plant-derived extracts such as *Sida cordata* [12], *Excoecaria agallocha* [13], and *Achyranthes japonica* [14], as well as microbial cultures like *Pseudomonas putida* [15], have been reported to mediate the synthesis of silver and zinc oxide nanoparticles.

In the present study, *Prunus avium L.* stem was utilized for the synthesis of silver nanoparticles. Previous studies have demonstrated that different parts of *Prunus avium L.*, particularly the stem, are rich in phenolic compounds and exhibit notable antibacterial, antioxidant, and anticancer activities. Notably, comparative analyses have shown that the antioxidant capacity of the stem is higher than that of the fruit, highlighting its potential for biomedical applications [16,17]. Here, we utilized an alcoholic extract of *P. avium L.* stem to reduce silver nitrate and synthesize AgNPs. Then, the biological activities of AgNPs@*PAS* were extensively evaluated. This study examined their antimicrobial, antioxidant, and anticancer properties, as well as their therapeutic efficacy in promoting burn wound healing.

2. Experimental

2.1. Materials

Silver nitrate, methanol and DMSO were purchased from Sigma-Aldrich (St. Louis, MO, USA). Deionized water was used as the solvent in all experimental procedures. In this study, three Gram-positive bacteria strains (*Staphylococcus aureus* (ATCC 29213), *Streptococcus mutans* (ATCC 35668), *Enterococcus faecalis* (ATCC 29212)) and two Gram-negative strains (*Escherichia coli* (ATCC 25922), *Klebsiella pneumoniae* (ATCC 9997)), fungal species *Candida albicans* (ATCC 10231), were obtained from the Pasteur Institute of Iran. Dulbecco's modified Eagle's medium (DMEM), trypsin-EDTA, penicillin-streptomycin, and fetal bovine serum (FBS) were obtained from BIO IDEA (Iran). The Zantox assay kit was supplied by Kavosh Arian Azma Company, while xylazine (2 %) and ketamine (10 %) were obtained from Alfasan. All experimental procedures were conducted in triplicate.

2.2. Preparation of Prunus avium L. stem extracts

The light-brown stems *Prunus avium L.* appears as slender, round branches. A total of 100 g of dried *P. avium* stems was mixed with 1 L of methanol, and the mixture was agitated on a shaker at 150 rpm for 72 h. The extraction process was performed away from direct sunlight to prevent degradation of light-sensitive phytochemicals. The mixture was then filtered. Subsequently, the filtrate was concentrated and dried in an oven at approximately 40 °C for 24 h. The obtained extract was kept at 4 °C.

2.3. Biosynthesis of AgNPs@PAS

Three key parameters were selected for the biosynthesis of AgNPs to identify the optimal conditions for producing AgNPs@*PAS*. According to previous studies, silver nanoparticles typically exhibit a characteristic surface plasmon resonance (SPR) absorption peak within the wavelength range of approximately 380–450 nm, which is closely associated with nanoparticle size and concentration [18,19]. Therefore, in this study, the optimal synthesis conditions were determined by comparing the SPR absorption peaks obtained under different reaction parameters.

2.3.1. Optimization of silver nitrate concentration

The *Prunus avium* stem extract was first adjusted to pH 12 using 1 M NaOH to activate phenolic functional groups. Subsequently, the pH-adjusted extract was added dropwise to the silver nitrate solution under continuous stirring. UV-Vis absorbance spectra were monitored for each reaction to determine the optimal silver nitrate concentration for AgNP synthesis.

2.3.2. Optimization of reaction time

After identifying the optimal silver nitrate concentration, the biosynthesis of AgNPs@*PAS* was evaluated at various contact times (15, 30, 45, and 60 min) in order to determine the most efficient duration for nanoparticle formation.

2.3.3. Optimization of reaction temperature

To determine the optimal temperature, the extract solution was added to the previously optimized silver nitrate concentration at room temperature, 55 °C, and 85 °C. At 85 °C, 15 mM $AgNO_3$ was dissolved in water (10 mL) under moderate stirring. Separately, 100 mg of *P. avium* stem extract was dissolved in 10 mL of deionized water, filtered, and adjusted to pH 12 using 1 M NaOH. The extract was then added dropwise to the above solution. A rapid color change indicated the successful preparation of silver nanoparticles. The reaction was allowed to proceed for 45 min. Following the reaction, UV-Vis spectra were recorded in the 300–500 nm range. The synthesized nanoparticles were collected and washed.

2.4. Characterization

Ultraviolet-visible (UV-Vis) absorption spectra were recorded using a NanoDrop spectrophotometer (BioTek Epoch, USA). Crystalline structure and phase identification of the synthesized nanomaterials were examined by X-ray diffraction (XRD) using a Philips PW 1800 diffractometer with Cu Kα radiation. Fourier-transform infrared (FT-IR) spectra were collected at ambient temperature employing a PerkinElmer Spectrum Two™ IR spectrometer (Model L160000U) in the range of 400–4000 cm^{-1} to identify surface functional groups. The hydrodynamic size distribution and zeta potential of the nanoparticles were determined by dynamic light scattering (DLS) using a NanoBrook 90Plus analyzer (Brookhaven Instruments, Model 18051, USA). Morphological characteristics were investigated by transmission electron microscopy (TEM) using a Zeiss EM10C operating at 100 kV, while field emission scanning electron microscopy (FESEM) coupled with energy-dispersive X-ray spectroscopy (EDS) was performed using a TESCAN BRNO Mira3 LMU system to further analyze surface morphology and elemental composition.

2.5. Antimicrobial properties of AgNPs@PAS

The antifungal and antibacterial activities of the *Prunus avium L.* stem extract and AgNPs@*PAS* were evaluated using the broth microdilution method. For MIC determination, 100 μL of various concentrations of AgNPs@*PAS* and the plant extract were added to a sterile 96-well microplate. A 0.5 McFarland standard was prepared for each microbial strain and subsequently diluted 1:150 in Mueller-Hinton broth. Then, 100 μL of the diluted microbial suspension was added to each well, resulting in a final inoculum of approximately 5×10^5 CFU per well. The microplates were incubated at 37 °C for 24 h. After incubation, all wells were examined visually for turbidity. The MIC was defined as the lowest

concentration of the sample at which visible microbial growth was inhibited, consistent with standard broth microdilution methodology [20].

2.6. Antioxidant capacity of AgNPs@PAS

The antioxidant performance was evaluated based on the DPPH radical scavenging assay. When dissolved in an organic solvent, the DPPH radical exhibits a purple color, which shifts to yellow in the presence of reducing agents (hydrogen donors). These changes are monitored spectrophotometrically at 517 nm. The extent of decrease in absorbance at this wavelength reflects the free radical scavenging activity of the sample. Results were presented in terms of the percentage of DPPH radical scavenging activity [21,22]. The scavenging activity was calculated using the following equation: Scavenging rate (%) $= (1\text{-}A_s/A_0) \times 100$; where A_s is the absorbance of the sample and A_0 is the absorbance of the blank solution. This approach allows the determination of the sample's radical-scavenging efficiency based on the measured absorbance values.

2.7. Cytotoxicity activity of AgNPs@PAS

The cytotoxic potential of AgNPs@*PAS* was evaluated using the MTT assay. Cells were maintained in T25 culture flasks containing Dulbecco's Modified Eagle Medium (DMEM) supplemented with 10 % fetal bovine serum (FBS) and 1 % penicillin/streptomycin and cultured at 37 °C in a humidified incubator with 5 % CO_2. Following 24 h of incubation, the medium was replaced with fresh DMEM containing various concentrations of AgNPs@*PAS* (3.25–200 μg/mL), and the cells were incubated for an additional 24 h. Thereafter, 10 μL of MTT solution (5 mg/mL) was added to each well and the plates were incubated for three hours. The supernatant was carefully removed, and 100 μL of DMSO was added to dissolve the resulting formazan crystals. Absorbance was measured at 570 nm, and cell viability was measured with the following equation:

Cell viability (%) = (Absorbance of sample/Absorbance of control) × 100

2.8. Formulation of an AgNPs@PAS-loaded Vaseline ointment

The AgNPs@*PAS* ointment was formulated by melting 1 g of Vaseline at 60 °C, followed by incorporation of 0.01 g (1 % w/w) of AgNPs@*PAS* under continuous mixing to obtain a homogeneous ointment.

2.9. In vivo experimental procedure in rat

2.9.1. Burn wound model

Twenty-four male Wistar rats (7–9 months old, 180–210 g) were obtained from the Center Experimental Studies and Laboratory Animals at Birjand University of Medical Sciences. Prior to experimentation, anesthesia was induced via intraperitoneal injections of xylazine (2 %, 10 mg/kg BW) and ketamine (10 %, 75 mg/kg BW) (Alfasan Co., Woerden, Holland). After achieving complete anesthesia, the dorsal hair of each rat was shaved. Burn wounds were created using an aluminum rod (1.8 cm diameter). The rod was heated in boiling water for 10 min and immediately applied to the dorsal skin for 20 s without exerting additional pressure. Two burn wounds were created on the dorsum of each rat. Photographs of the wounds were taken immediately after injury. The rats were randomly divided into four groups (n = 6 each): (i) Positive control: treated with 1 % silver sulfadiazine (Emad Darman Pars Co., Saveh, Iran); (ii) AgNPs@*PAS* ointment group: treated with 1 % AgNPs@*PAS* Vaseline ointment; (iii) Vaseline group: treated with Vaseline alone (ointment base); (iv) Negative control: received no treatment.

2.9.2. Evaluation of burn wound closure

Digital images of the wounds were captured on days 3, 7, and 14 post-injury. The extent of wound closure was expressed as a percentage and calculated according to the following equation:

Wound closure (%) = [(initial wound area - wound area on the specified day) / initial wound area] × 100

2.10. Data analysis

All statistical evaluations were carried out using SPSS software (version 19.0; Chicago, IL, USA). Data were analyzed by one-way analysis of variance (ANOVA) or the Kruskal-Wallis test for non-parametric datasets. In addition, ImageJ software was employed to measure wound areas and determine the percentage of wound closure.

3. Results and discussion

3.1. UV-Vis

UV-Vis spectrophotometry was utilized to confirm the preparation of AgNPs@*PAS* and to evaluate the effects of three key synthesis parameters: silver nitrate concentration, contact time, and temperature. The formation of AgNPs was initially indicated by a visible color change which results from the SPR of silver nanoparticles [23,24]. Silver nitrate concentration played a critical role in nanoparticle formation. As shown in Fig. 1a, increasing the $AgNO_3$ concentration from 5 to 15 mM led to a marked increase in SPR peak intensity, reflecting enhanced nanoparticle formation. However, further increasing the concentration to 20 mM resulted in a decrease in peak intensity, likely attributable to nanoparticle aggregation at higher ionic strength. The effect of reaction time is illustrated in Fig. 1b. Extending the reaction duration from 15 to 45 min progressively increased the SPR peak intensity, indicating more efficient nanoparticle synthesis. Beyond 45 min, no substantial change was observed at 60 min, suggesting that the reaction had reached completion. As depicted in Fig. 1c, increasing the reaction temperature enhanced AgNP formation, with the strongest and sharpest SPR peak observed at 85 °C. This indicates that 85 °C served as the optimal temperature for the green synthesis of AgNPs@*PAS* under the conditions examined.

3.2. XRD analysis

XRD was performed to evaluate the crystalline structure of the synthesized AgNPs@*PAS*. The diffraction pattern is shown in Fig. 2. The AgNPs@*PAS* exhibited distinct diffraction peaks at 2θ values of 38.03°, 44.18°, 64.43°, and 77.18°, corresponding to the (111), (200), (220), and (311) planes. Comparison of this pattern with the standard JCPDS silver file (01–087–0717) confirmed that the synthesized nanoparticles matched the characteristic fcc structure of metallic silver. In addition to the primary Ag peaks, several minor peaks appeared at approximately 28°, 32°, 46°, 55°, and 57°, which are attributed to silver chloride. This impurity likely resulted from trace chloride ions present in the distilled water or chloride ions in the aqueous extract used during synthesis, leading to partial AgCl precipitation [25]. The XRD peaks observed in this study closely match those reported by Said et al., in which AgNPs showed characteristic reflections at 38.1°, 44.2°, 64.4°, and 77.2° [26]. Similarly, the XRD results of Mehta et al.'s synthesized silver nanoparticles were consistent with the present findings [27]. Together, these results confirm that the *Prunus avium* stem extract effectively reduced Ag^+ ions and facilitated the fabrication of crystalline silver nanoparticles.

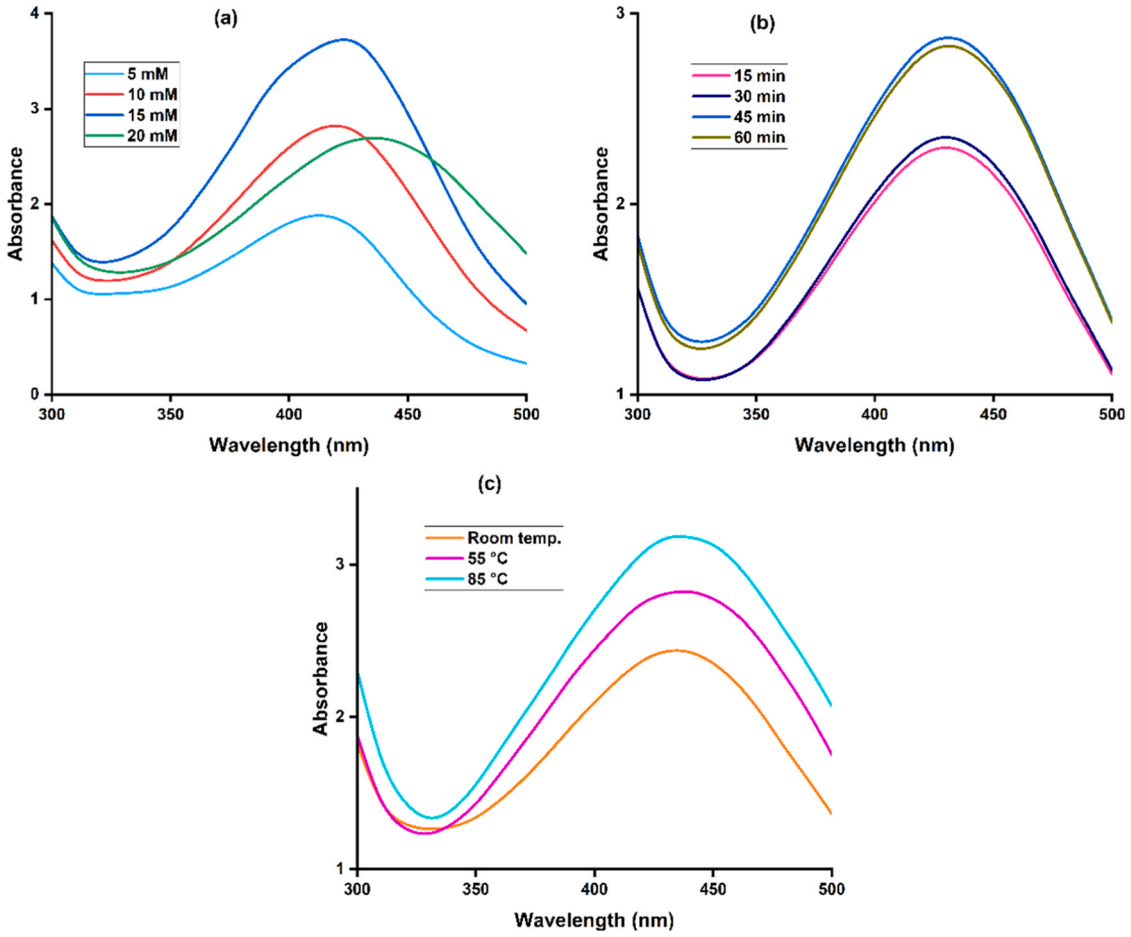

Fig. 1. The UV-Vis spectrophotometry analysis of different parameters, including a) silver nitrate concentration, b) reaction time, and c) reaction temperature.

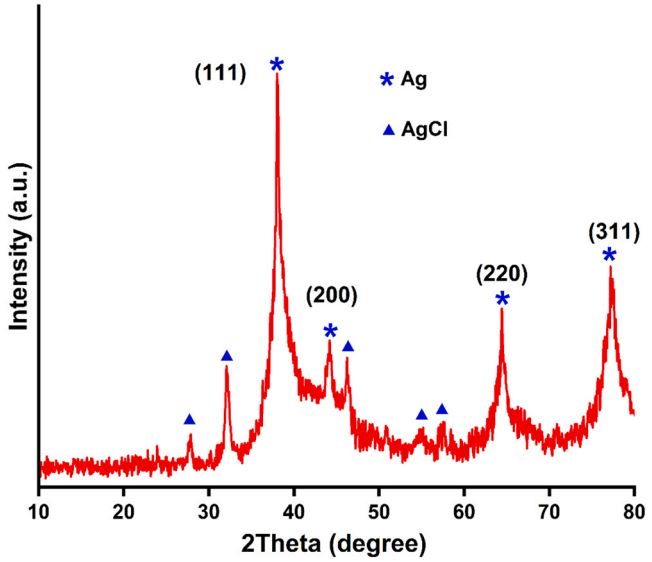

Fig. 2. XRD pattern of AgNPs@*PAS*.

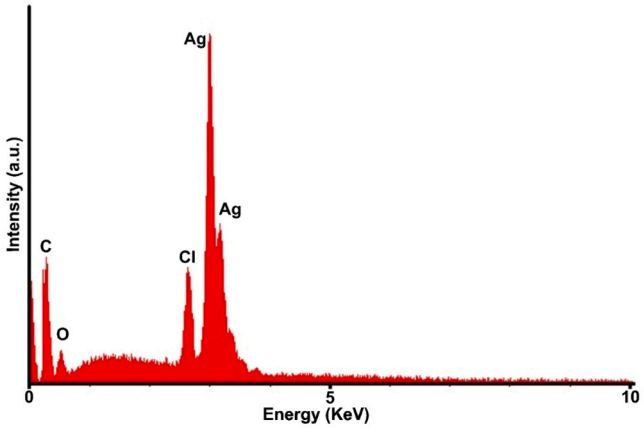

Fig. 3. The EDS spectrum of AgNPs@*PAS*.

3.3. EDS, FESEM and TEM analysis

EDS was employed to determine the elemental composition of AgNPs@*PAS* (Fig. 3). A strong characteristic Ag peak appeared at approximately 3 keV, confirming the presence of silver in the synthesized nanoparticles. In addition, peaks corresponding to chlorine (Cl), carbon (C) and oxygen (O) were detected, which originate from the phytochemical constituents of the *Prunus avium L.* stem extract adhering to the nanoparticle surface. Similar strong Ag signals around 3 keV have been reported for other green-synthesized AgNPs [28]. A chlorine peak was also observed, consistent with the XRD findings, and is attributed to the partial formation of silver chloride during synthesis. The morphology and surface structure of the nanoparticles were further evaluated using FESEM (Fig. 4a). The FESEM images revealed aggregated spherical nanoparticles, with irregular clustering likely caused by plant-derived capping and stabilizing agents coating the AgNPs@*PAS*.

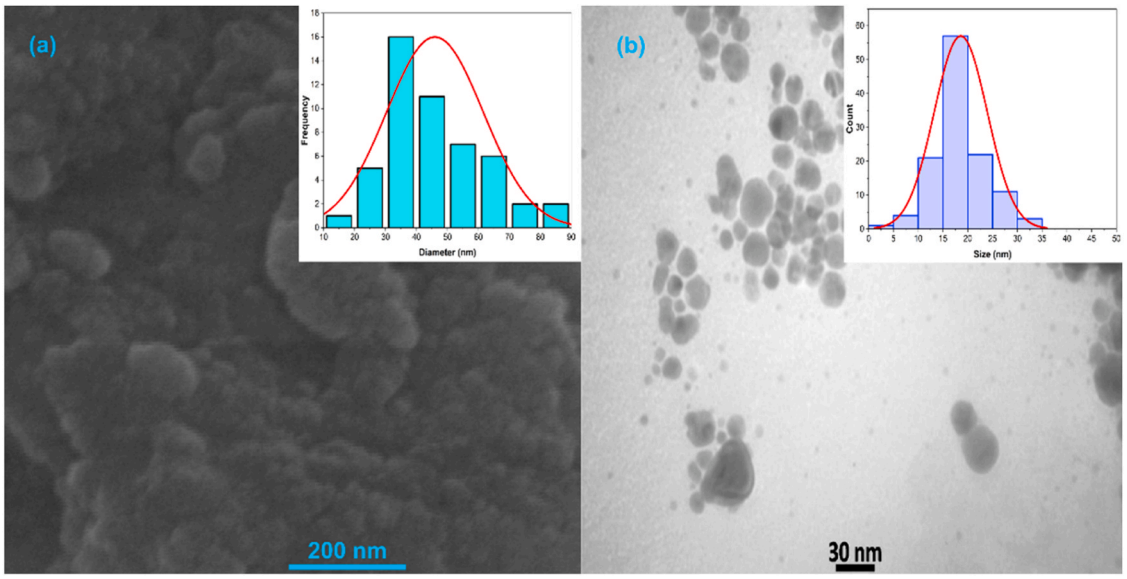

Fig. 4. The (a) FESEM and (b) TEM images of AgNPs@*PAS*.

To further investigate nanoparticle morphology and size distribution, TEM analysis was conducted. The TEM images (Fig. 4b) confirmed that the AgNPs@*PAS* exhibited a predominantly spherical morphology, with particle sizes mainly in the range of 10–35 nm. A difference was observed between the particle size distributions obtained from FESEM and TEM analyses. The larger apparent particle sizes in FESEM can be attributed to particle agglomeration and surface effects, whereas TEM provides a more accurate estimation of individual nanoparticle core sizes.

3.4. DLS and zeta potential analysis

The hydrodynamic size reflects the size of the nanoparticle together with the solvation layer and any adsorbed phytochemicals, and therefore it is typically larger than the physical core size observed by TEM [29]. The average hydrodynamic diameter of AgNPs@*PAS* was measured to be 79.2 nm (Fig. 5a). This value is consistent with previous reports of bio-fabricated AgNPs, such as the findings of Khane et al., who reported a hydrodynamic diameter of 82.51 nm [30]. As shown in Fig. 5b, the zeta potential of AgNPs@*PAS* was + 21.16 mV. A zeta potential in this range indicates moderate electrostatic stability, suggesting

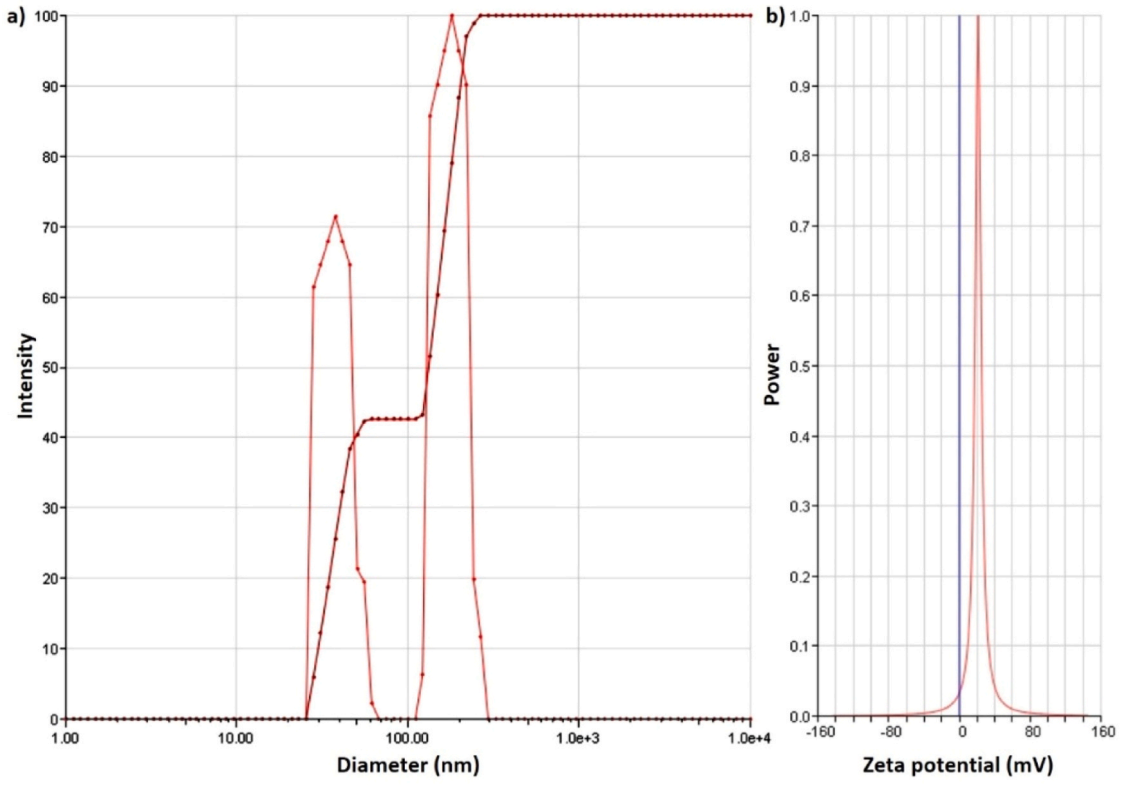

Fig. 5. The a) DLS analysis and b) zeta potential of synthesized AgNPs@*PAS*.

that the nanoparticles possess sufficient surface charge (likely derived from phytochemical capping agents) to maintain a relatively stable dispersion under the tested conditions [30].

3.5. FT-IR

FT-IR technique was carried out to identify the functional groups present in the *Prunus avium L.* stem extract and the synthesized AgNPs@*PAS* (Fig. 6). The FT-IR spectrum of the plant extract (Fig. 6a) exhibited characteristic absorption bands at 3380, 2926, 2854, 1712, 1637, 1452, 1269, and 1052 cm^{-1}. The broad band at 3380 cm^{-1} corresponds to O-H stretching vibrations groups present in phenolic compounds [31]. The peaks at 2926 and 2854 cm^{-1} are attributed to C-H stretching vibrations of aliphatic groups. The strong absorption at 1712 cm^{-1} corresponds to C═O stretching of carbonyl functional groups. The band at 1637 cm^{-1} is typically assigned to C═C or C-O stretching in aromatic rings or phenolic structures [32]. Additionally, the peaks at 1452, 1269, and 1052 cm^{-1} represent CH_2/CH_3 bending, C-O stretching in phenolic compounds, and C-O stretching vibrations, respectively [33]. The FT-IR spectrum of AgNPs@*PAS* (Fig. 6b) displayed similar bands at 3401, 2919, 2850, 1689, 1600, 1450, 1377, 1255, and 1045 cm^{-1}. Similarities in the FT-IR spectra of the extract and AgNPs@*PAS* provide evidence for the attachment of plant-derived functional groups to the nanoparticle surface. This observation suggests that phytochemicals in the *P. avium* stem extract acted both as reducing and capping agents, reducing Ag^+ ions to Ag^0 during synthesis and subsequently stabilizing the nanoparticles by adsorbing onto their surfaces [34]. Similar findings were reported by Sultan et al., who attributed the resemblance between the FT-IR spectra of green-synthesized AgNPs and their corresponding plant extract to the involvement of plant metabolites in nanoparticle reduction and stabilization [32].

3.6. Antimicrobial activity

Table 1 summarizes the antifungal and antibacterial activities of AgNPs@*PAS*, and *Prunus avium L.* stem extract against gram-negative, gram-positive bacteria, and the fungal strain *C. albicans*. While the *P. avium* stem extract exhibited negligible antibacterial activity even at high concentrations (1000 μg/mL), AgNPs@*PAS* effectively inhibited the proliferation of all tested microorganisms. Among the bacterial species examined, AgNPs@*PAS* showed the strongest antibacterial activity against *E. coli* (MIC= 35 μg/mL), while the weakest activity was observed against *S. aureus* (MIC= 70 μg/mL). Notably, AgNPs@*PAS* exhibited pronounced antifungal activity against *C. albicans*, with an MIC value of 17.5 μg/mL, indicating higher sensitivity of the fungal strain compared to the tested bacteria. Comparable antifungal performance has been reported by Zare-Bidaki et al., who synthesized green AgNPs using *Petroselinum crispum* seeds and reported an MIC value of 15.62 μg/mL against *C. albicans* [35]. In another study, Yildirim et al. synthesized AgNPs via a green method using *Prunus avium* fruit extract and demonstrated antibacterial activity against *S. aureus* and *E. faecalis* using the disk diffusion assay [36]. The antimicrobial performance of silver nanoparticles is widely recognized to be dependent on their physicochemical properties, particularly particle size and surface area. Smaller nanoparticles with larger surface-to-volume ratios exhibit

Table 1
The MIC/MBC/MFC results of AgNPs@*PAS* and *Prunus avium L.* stem extract.

Microorganism	AgNPs@*PAS*		*Prunus avium L.* stem extract	
	MIC (μg/mL)	MBC/MFC (μg/mL)	MIC (μg/mL)	MBC/MFC (μg/mL)
E. coli	35	140	>1000	>1000
K. pneumoniae	35	280	>1000	>1000
S. aureus	70	280	>1000	>1000
S. mutans	35	280	>1000	>1000
E. faecalis	70	140	>1000	>1000
C. albicans	17.5	70	>1000	>1000

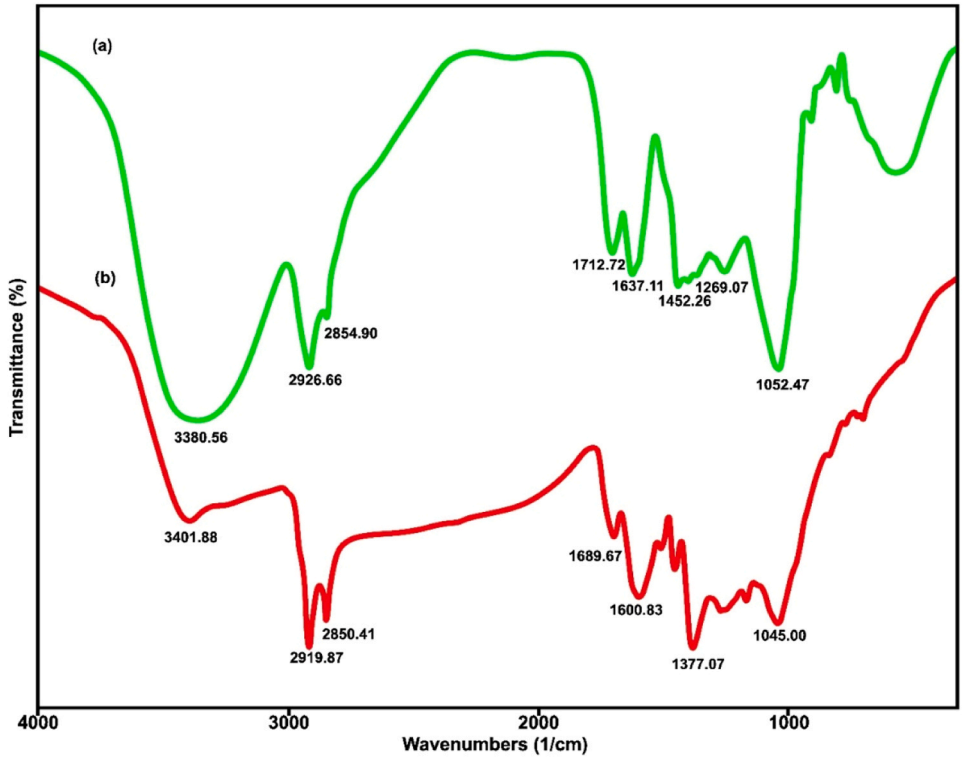

Fig. 6. FT-IR analysis of (a) *Prunus avium L.* stem extract and (b) AgNPs@*PAS*.

enhanced antimicrobial performance due to increased interaction with microbial cell membranes and facilitated cellular penetration [36]. Although the exact antimicrobial mechanisms of silver nanoparticles have not been fully elucidated, multiple pathways have been proposed. AgNPs can attach to microbial cell membranes, where the gradual release of Ag^{+} ions disrupts membrane integrity, interferes with ion transport, and compromises osmotic balance [37]. Membrane disruption may lead to leakage of intracellular components and allow nanoparticles to penetrate into the cell. Once internalized, AgNPs can interact with proteins, enzymes, and DNA, thereby inhibiting essential cellular processes and cell proliferation [38]. Additionally, AgNPs are capable of generating ROS, which further damage cellular components and contribute to microbial cell death [39]. Effective control of microbial infections remains a major challenge in burn wound management [40]. Common pathogens associated with chronic burn wound infections include *P. aeruginosa, Streptococcus spp.*, *Klebsiella spp.*, *Enterococcus spp.*, *S. aureus*, and *E. coli*, while *Candida spp.* are among the predominant fungal pathogens [40].

3.7. Analysis of antioxidant properties

Oxidative stress, caused by disrupted equilibrium between free radicals and antioxidants, plays a key role in many chronic pathological conditions, increasing interest in antioxidants that can mitigate cellular injury. Compounds exhibiting antioxidant activity reduce cellular damage by neutralizing free radicals via electron transfer mechanisms [41]. The antioxidant properties of AgNPs@*PAS* and *Prunus avium L.* stem extract was investigated using the DPPH radical scavenging assay. The results are presented in Fig. 7. The *P. avium* stem extract exhibited concentration-dependent antioxidant activity, achieving approximately 30 % DPPH inhibition at 1 mg/mL, which increased to 85 % at 6.25 mg/mL. Notably, AgNPs@*PAS* demonstrated significantly higher antioxidant activity than the plant extract alone. At a concentration of 140 μg/mL, AgNPs@*PAS* achieved 93 % DPPH radical scavenging, indicating a strong free radical neutralization capacity. Overall, both the extract and AgNPs@*PAS* showed a dose-dependent increase in DPPH inhibition. Plant extracts are known to contain various antioxidant compounds, particularly phenolic constituents, which contribute to their free radical scavenging activity. Previous studies have reported that *Prunus avium L.* stems extract contains flavonoids, tannins, and catechin, all of which possess notable antioxidant properties [16]. Consistently, FT-IR analysis in the present study revealed functional groups associated with phenolic and antioxidant compounds, supporting the observed antioxidant properties of the extract. In the green synthesis method, the antioxidant property of AgNPs, along with the antioxidant properties of the plant extract, enhances the overall antioxidant property of the biosynthesized nanoparticles [30]. For instance, Baran et al. reported that green-synthesized AgNPs using *Allium cepa L.* peel extract achieved 50 % DPPH inhibition at a concentration of 151.3 μg/mL [42]. Similarly, Khane et al. observed 50 % DPPH inhibition at 42.5 μg/mL for AgNPs synthesized using *Citrus limon* zest extract [30]. Variations in antioxidant activity among green-synthesized AgNPs are commonly attributed to differences in particle size, surface chemistry, and the nature of phytochemical capping agents. Given the established role of oxidative stress in delayed wound healing, antioxidant-rich materials are of particular interest for wound care applications [43,44]. The pronounced antioxidant activity of AgNPs@*PAS* (93 % inhibition at 140 μg/mL) suggests that these nanoparticles may effectively mitigate oxidative stress in wound environments and contribute to improved tissue regeneration.

3.8. Anticancer activity

The cytotoxic effect of AgNPs@*PAS* on a human breast cancer cell line was investigated using the MTT assay. Following 24 h of treatment with different concentrations of AgNPs@*PAS* (12.5–200 μg/mL), cell viability was determined. The results are presented in Fig. 8. The MTT assay revealed a concentration-dependent reduction in cell viability following treatment with AgNPs@*PAS*. MCF-7 cell viability declined to 21.2 % at the maximum evaluated concentration of 200 μg/mL. According to the dose-response curve, the IC_{50} of AgNPs@*PAS* was determined to be 78.8 μg/mL, confirming its cytotoxic activity toward MCF-7 cells. Consistent with the present findings, Jang et al. [45] and Khorrami et al. [9] reported that silver nanoparticles synthesized via green methods effectively reduced the viability of MCF-7 cells in vitro. In contrast, Al-Sheddi et al. reported a lower IC_{50} value (32 μg/mL) for green silver nanoparticles against the same cell line [46]. Such variations in cytotoxic efficacy among green-synthesized AgNPs may be attributed to differences in particle size, morphology, surface chemistry,

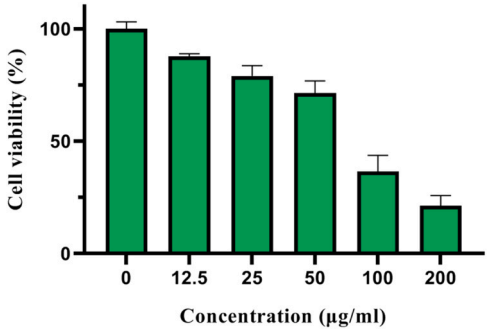

Fig. 8. The MTT test of various concentration of AgNPs@*PAS* against MCF-7 cell lines.

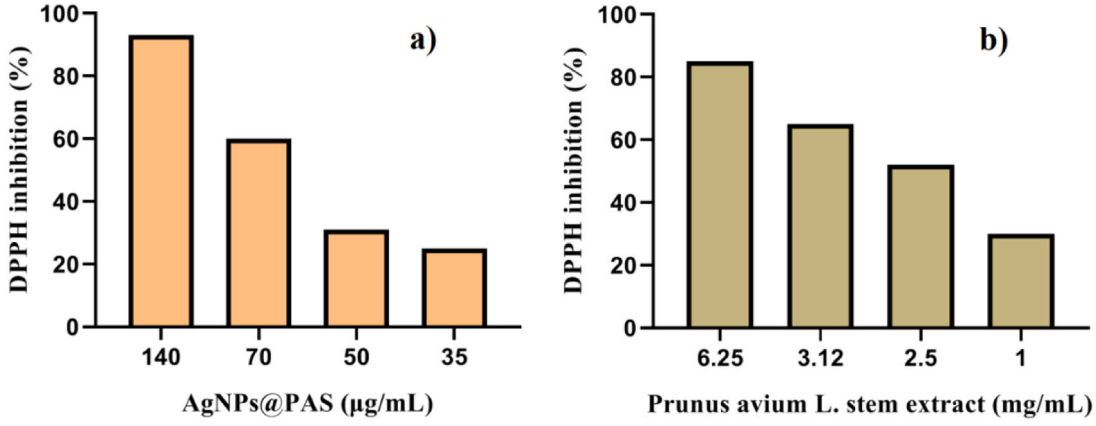

Fig. 7. The DPPH antioxidant analysis of a) AgNPs@*PAS* and b) *Prunus avium L.* stem extract.

and the nature of phytochemical capping agents. Similarly, Hashemabadi et al. synthesized AgNPs using *Prunus avium* gum extract and demonstrated cytotoxic effects against the MCF-7 cell line at concentrations as low as 50 μg/mL. MTT assay results demonstrated the cytotoxic effects of AgNPs on MCF-7 cell line at doses of 50 μg/mL. Their gene expression analysis further revealed increased Bax and decreased Bcl-2 mRNA levels, indicating activation of apoptosis following AgNP treatment [47]. The anticancer mechanisms of silver nanoparticles are believed to involve multiple pathways. Studies suggest that the release of silver ions (Ag^{+}) from nanoparticles leads to increased intracellular reactive ROS generation, which induces oxidative stress and damages cellular components such as DNA, proteins, and enzymes [48,49]. AgNPs have been implicated in the activation of apoptotic pathways via increased expression of pro-apoptotic markers (BAX, P53, and caspase-3) and simultaneous downregulation of anti-apoptotic components [50–52]. Supporting these findings, Alharbi et al. demonstrated that AgNPs could induce apoptosis in cancer cells and arrest the cell cycle by causing irreversible DNA damage [53]. The observed differences in the anticancer activity of AgNPs can be related to variations in particle size, morphology, and surface functionalization. Numerous studies have illustrated that the cytotoxic potential of AgNPs is strongly influenced by their size and shape [54,55], with smaller nanoparticles generally exhibiting enhanced cytotoxicity due to increased cellular uptake and higher surface reactivity [55]. In addition, nanoparticle morphology can affect cellular internalization pathways, thereby influencing biological responses [55]. Plant-mediated silver nanoparticles are generally spherical in morphology and have been reported to display notable anticancer effects across different cancer cell lines [54]. Furthermore, Khorrami et al. reported that bio-fabricated AgNPs exhibited significantly stronger anticancer activity than both the corresponding plant extract and commercially produced AgNPs, which was attributed to synergistic effects arising from phytochemical capping agents on the nanoparticle surface [9].

3.9. Evaluation of wound closure percentage

As illustrated in Fig. 9a, a Vaseline-based ointment containing 1 % AgNPs@*PAS* was prepared. According to the experimental protocol

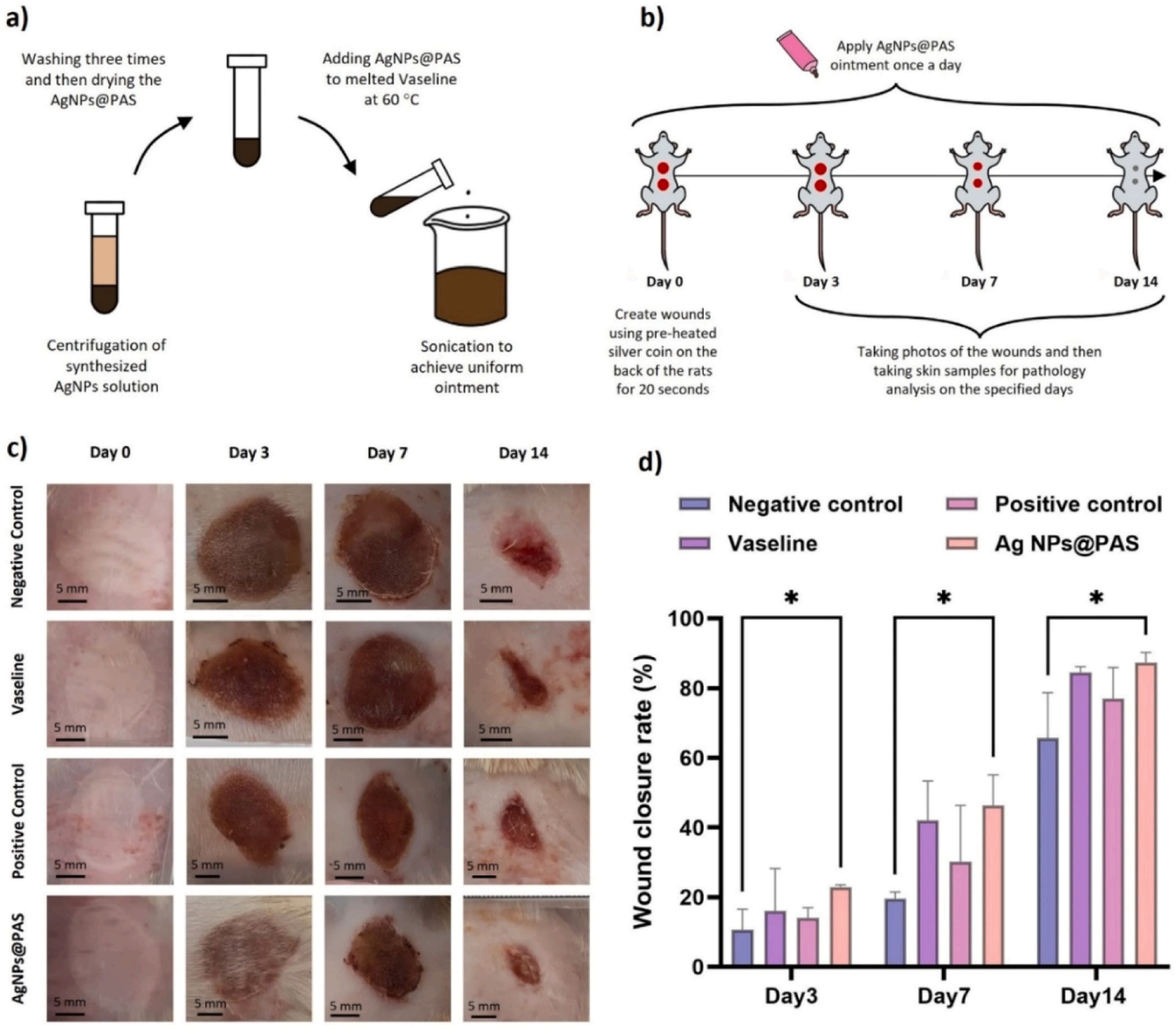

Fig. 9. The schematic of a) Vaseline-based ointment preparation and b) cutaneous burn wound model procedures. c) The wound images in specific days. d) The wound closure rate of different wound in specific days (* $P < 0.05$).

shown in Fig. 9b, the ointment was applied topically to the burn wounds for 14 days, and wound sampling and imaging were performed on predetermined days. Representative images of burn wounds from each experimental group are presented in Fig. 9c. The wound closure percentage, calculated using Digimizer software, is shown in Fig. 9d. On day 3, the AgNPs@*PAS*-treated group exhibited a significantly higher wound closure rate compared with the negative control group. The AgNPs@*PAS* group exhibited an increased wound closure rate relative to the positive control; however, this difference was not statistically significant. Similarly, on days 7 and 14, wound closure in the AgNPs@*PAS*-treated group remained significantly greater than in the negative control group, while no statistically significant difference was observed when compared with the positive control. Excessive production of ROS can lead to oxidative stress, which damages cells and prolongs inflammation, thereby impairing the wound healing process. Compounds with antioxidant activity may contribute to wound repair by reducing oxidative stress within the wound microenvironment [43]. In addition, AgNPs are known to exhibit antimicrobial properties that may help reduce the risk of wound infection [56]. Previous studies have suggested that AgNPs may modulate inflammatory responses and support tissue regeneration by influencing processes such as angiogenesis, collagen deposition, and fibroblast proliferation, all of which are critical for effective wound healing [57]. For example, Mukhtarovna et al. investigated the effects of bio-fabricated AgNPs in a rabbit wound model and reported enhanced wound closure, improved re-epithelialization, and increased collagen deposition compared with untreated controls [58]. Recent studies have further highlighted the potential of green-synthesized AgNPs in accelerating burn wound healing. *Anethum graveolens* seed-mediated AgNPs were shown to promote wound closure within 14 days [29], while *Petroselinum crispum* seed-derived AgNPs significantly enhanced wound closure rates compared with negative control and Vaseline-treated groups after 7 and 14 days [35]. Wound healing effects of bio-fabricated AgNPs are generally linked to synergistic antibacterial, antioxidant, and anti-inflammatory actions, together with their supportive role in collagen deposition, fibroblast activity, and angiogenesis [59,60]. Consistent with this, Lakkim et al. demonstrated that AgNPs fabricated using natural extracts promoted wound healing in BALB/c mice, as evidenced by reduced scar width, improved epithelial regeneration, finer collagen organization, and decreased inflammatory cell infiltration in histopathological analyses [61]. In the present study, the enhanced wound closure observed in the AgNPs@*PAS*-treated group may be associated with the antimicrobial and antioxidant properties of the nanoparticles, which could help limit infection and inflammation at the wound site. While the applied dose (1 % w/w in Vaseline) appeared effective in promoting wound closure, further dose-response studies are required to determine the optimal and safest therapeutic concentration for future clinical applications.

4. Conclusion

In this work, *Prunus avium L.* stem extract was applied as a green reducing agent for the successful synthesis of silver nanoparticles. The resulting AgNPs@*PAS* exhibited suitable physicochemical characteristics and demonstrated multifunctional biological activities, including antimicrobial, antioxidant, and moderate anticancer effects in vitro. In vivo evaluation further revealed enhanced burn wound closure in AgNPs@*PAS*-treated groups compared with untreated controls. These findings suggest that *P. avium* stem-mediated AgNPs may serve as a promising multifunctional nanomaterial for wound-related biomedical applications. However, further investigations focusing on dose optimization, long-term toxicity, and pharmacokinetics are required prior to clinical translation.

CRediT authorship contribution statement

Pouria Mohammadparast-Tabas: Writing – original draft, Visualization, Validation, Investigation, Formal analysis, Conceptualization. **Alireza Ghasempour:** Writing – original draft, Visualization, Investigation. **Hamideh Dehghan:** Writing – original draft, Visualization, Validation, Investigation, Formal analysis. **Majid Zare-Bidaki:** Writing – review & editing, Validation, Supervision, Project administration, Methodology, Formal analysis, Conceptualization. **Mortazavi-derazkola Sobhan:** Writing – review & editing, Visualization, Validation, Supervision, Project administration, Methodology, Data curation, Conceptualization. **Fatemeh Sadat Nabavi sales:** Writing – original draft. **Alemeh Gholami:** Writing – original draft. **Yasaman Soleimanmanesh:** Writing – original draft, Investigation. **Marzieh Jafari Bidhendi:** Writing – original draft.

Funding

No financial support was received for the study.

Declaration of Competing Interest

The authors declare that they have no known competing financial interests or personal relationships that could have appeared to influence the work reported in this paper.

Acknowledgement

This research is the result of research with ethical code IR.BUMS.REC.1401.128. We are grateful to Birjand University of Medical Sciences for supporting this research.

Data availability

Data will be made available on request.

References

[1] H.M. Mehwish, G. Liu, M.S.R. Rajoka, H. Cai, J. Zhong, X. Song, L. Xia, M. Wang, R. M. Aadil, M. Inam-Ur-Raheem, Y. Xiong, H. Wu, M.I. Amirzada, Q. Zhu, Z. He, Therapeutic potential of Moringa oleifera seed polysaccharide embedded silver nanoparticles in wound healing, Int. J. Biol. Macromol. 184 (2021) 144–158.
[2] X. Wang, K. Sun, C. Wang, M. Yang, K. Qian, B. Ye, X. Guo, Y. Shao, C. Chu, F. Xue, J. Li, J. Bai, Ultrasound-responsive microfibers promoted infected wound healing with neuro-vascularization by segmented sonodynamic therapy and electrical stimulation, Biomaterials 313 (2025) 122803.
[3] H. Dehghan, M. Sedighi, A.M. Jafari-Nozad, S. Jafari, E. Alemzadeh, T. Farkhondeh, S. Samarghandian, Gold nanoparticles and wound healing in rodents: a systematic study, Curr. Nanosci. 19 (2023) 840–849.
[4] A. Ghasempour, H. Dehghan, M. Mahmoudi, F. Lavi Arab, Biomimetic scaffolds loaded with mesenchymal stem cells (MSCs) or MSC-derived exosomes for enhanced wound healing, Stem Cell Res. Ther. 15 (2024) 406.
[5] X.-F. Zhang, Z.-G. Liu, W. Shen, S. Gurunathan, Silver nanoparticles: synthesis, characterization, properties, applications, and therapeutic approaches, Int. J. Mol. Sci. 17 (2016) 1534.
[6] K.M.M. Abou El-Nour, Aa Eftaiha, A. Al-Warthan, R.A.A. Ammar, Synthesis and applications of silver nanoparticles, Arab. J. Chem. 3 (2010) 135–140.
[7] H.D. Beyene, A.A. Werkneh, H.K. Bezabh, T.G. Ambaye, Synthesis paradigm and applications of silver nanoparticles (AgNPs), a review, Sustain. Mater. Technol. 13 (2017) 18–23.
[8] F. Fatima, M.F. Aldawsari, M.M. Ahmed, M.K. Anwer, M. Naz, M.J. Ansari, A. M. Hamad, A. Zafar, M. Jafar, Green synthesized silver nanoparticles using tridax procumbens for topical application: excision wound model and histopathological studies, Pharmaceutics 13 (2021) 1754.
[9] S. Khorrami, A. Zarrabi, M. Khaleghi, M. Danaei, M.R. Mozafari, Selective cytotoxicity of green synthesized silver nanoparticles against the MCF-7 tumor cell line and their enhanced antioxidant and antimicrobial properties, Int. J. Nanomed. 13 (2018) 8013–8024.
[10] V. Lakkim, M.C. Reddy, R.R. Pallavali, K.R. Reddy, C.V. Reddy, A.L. Inamuddin, D. Bilgrami, Lomada, Green Synthesis of Silver Nanoparticles and Evaluation of Their Antibacterial Activity against Multidrug-Resistant Bacteria and Wound Healing Efficacy Using a Murine Model, Antibiotics 9 (2020) 902.
[11] S. Iravani, H. Korbekandi, S.V. Mirmohammadi, B. Zolfaghari, Synthesis of silver nanoparticles: chemical, physical and biological methods, Res. Pharm. Sci. 9 (2014) 385–406.
[12] B. Ravi, G. Mani, H. Pushparaj, H.T. Jang, V. Manickam, Sida cordata assisted bio-inspired silver nanoparticles and its antimicrobial, free-radical scavenging,

tyrosinase inhibition, and photocatalytic activity (4 in 1 system), Part. Sci. Technol. 41 (2023) 626–639.
[13] M.S. Khan, P.P. Dhavan, B.L. Jadhav, N.G. Shimpi, Ultrasound-assisted green synthesis of Ag-decorated ZnO nanoparticles UsingExcoecaria agallochaLeaf extract and evaluation of their photocatalytic and biological activity, ChemistrySelect 5 (2020) 12660–12671.
[14] B.O. Gadgeppa, B.M. Raman, G. Mani, G.P. Sidram, S.S. Pandit, J. Jaybalan, K. Kaliappan, H. Pushparaj, J. Hyun Tae, Phytogenic synthesis of silver nanoparticles using Achyranthes japonica root and its in vitro antimicrobial, antioxidant, and mushroom tyrosinase inhibitions, Part. Sci. Technol. 42 (2024) 107–119.
[15] J. Jayabalan, G. Mani, N. Krishnan, J. Pernabas, J.M. Devadoss, H.T. Jang, Green biogenic synthesis of zinc oxide nanoparticles using Pseudomonas putida culture and its In vitro antibacterial and anti-biofilm activity, Biocatal. Agric. Biotechnol. 21 (2019) 101327.
[16] Z. Ademović, S. Hodžić, Z. Halilić-Zahirović, D. Husejnagić, J. Džananović, B. Šarić-Kundalić, J. Suljagić, Phenolic compounds, antioxidant and antimicrobial properties of the wild cherry (Prunus avium L.) stem, Acta Period. Technol. (2017) 1–13.
[17] C. Bastos, L. Barros, M. Dueñas, R.C. Calhelha, M.J.R.P. Queiroz, C. Santos-Buelga, I.C.F.R. Ferreira, Chemical characterisation and bioactive properties of Prunus avium L.: the widely studied fruits and the unexplored stems, Food Chem. 173 (2015) 1045–1053.
[18] M. Alim-Al-Razy, G.M. Asik Bayazid, R.U. Rahman, R. Bosu, S.S. Shamma, Silver nanoparticle synthesis, UV-Vis spectroscopy to find particle size and measure resistance of colloidal solution, J. Phys. Conf. Ser. 1706 (2020) 012020.
[19] M. Sikder, J.R. Lead, G.T. Chandler, M. Baalousha, A rapid approach for measuring silver nanoparticle concentration and dissolution in seawater by UV–Vis, Sci. Total Environ. 618 (2018) 597–607.
[20] I. Wiegand, K. Hilpert, R.E. Hancock, Agar and broth dilution methods to determine the minimal inhibitory concentration (MIC) of antimicrobial substances, Nat. Protoc. 3 (2008) 163–175.
[21] H. Yousaf, A. Mehmood, K.S. Ahmad, M. Raffi, Green synthesis of silver nanoparticles and their applications as an alternative antibacterial and antioxidant agents, Materials Science Engineering C 112 (2020) 110901.
[22] B. Zamani Ranjbar Garmroodi, M. Rajabi Moghadam, A. Zarban, M. Bideh, Hepatoprotective effects of medicinal honey: introducing a new classification based on phenolic content and antioxidant capacity, J. Food Biochem. 2024 (2024) 4475104.
[23] A. Bazrgaran, S. Mahmoodabadi, A. Ghasempour, E. Shafaie, A. Sahebkar, S. Eghbali, Facile bio-genic synthesis of Astragalus sarcocolla (Anzaroot) gum extract mediated silver nanoparticles: characterizations, antimicrobial and antioxidant activities, Plant Nano Biol. 6 (2023) 100052.
[24] M. Zare-Bidaki, F.S. Nabavi Sales, A. Yousefinia, P. Mohammadparast-Tabas, H. Aramjoo, M. Torabi, S. Mortazavi-Derazkola, S.M. Ghoreishi, Exploring anticancer, antifungal, antibacterial, and antioxidant properties colchicum luteum root-mediated silver nanoparticles with green synthesis, Plasmonics 20 (2025) 4589–4603.
[25] D. Somda, J.L. Bargul, J.M. Wesonga, S.W. Wachira, Green synthesis of Brassica carinata microgreen silver nanoparticles, characterization, safety assessment, and antimicrobial activities, Sci. Rep. 14 (2024) 29273.
[26] A. Said, M. Abu-Elghait, H.M. Atta, S.S. Salem, Antibacterial activity of green synthesized silver nanoparticles using lawsonia inermis against common pathogens from urinary tract infection, Appl. Biochem. Biotechnol. 196 (2024) 85–98.
[27] B.K. Mehta, M. Chhajlani, B.D. Shrivastava, Green synthesis of silver nanoparticles and their characterization by XRD, J. Phys. Conf. Ser. 836 (2017) 012050.
[28] M. Shirzadi-Ahodashti, Z.M. Mizwari, Z. Hashemi, S. Rajabalipour, S.M. Ghoreishi, S. Mortazavi-Derazkola, M.A. Ebrahimzadeh, Discovery of high antibacterial and catalytic activities of biosynthesized silver nanoparticles using C. fruticosus (CF-AgNPs) against multi-drug resistant clinical strains and hazardous pollutants, Environ. Technol. Innov. 23 (2021) 101607.
[29] M. Zare-Bidaki, P. Mohammadparast-Tabas, M. Khorashadizade, P. Mohammadparast-Tabas, E. Alemzadeh, A. Saberi, H. Kabiri-Rad, S. Eghbali, Bio-synthesized AGS@AgNPs for wound healing, antioxidant support, antibacterial defense, and anticancer intervention, Biocatal. Agric. Biotechnol. 61 (2024) 103402.
[30] Y. Khane, K. Benouis, S. Albukhaty, G.M. Sulaiman, M.M. Abomughaid, A.Al Ali, D. Aouf, F. Fenniche, S. Khane, W. Chaibi, A. Henni, H.D. Bouras, N. Dizge, Green synthesis of silver nanoparticles using aqueous citrus limon zest extract: characterization and evaluation of their antioxidant and antimicrobial properties, Nanomaterials 12 (2022) 2013.
[31] D.F. Katowah, B.A. Almalki, Fabrication of a green nanocomposite film-based polylactic acid loaded cellulose acetate-Ag nanoparticles-curcumin nanoparticles for enhanced antibacterial activities, Egypt. J. Chem. 67 (2024) 377–387.
[32] M. Sultan, M. Siddique, R. Khan, A.M. Fallatah, N. Fatima, I. Shahzadi, U. Waheed, M. Bilal, A. Ali, A.M. Abbasi, Ligustrum lucidum leaf extract-assisted green synthesis of silver nanoparticles and nano-adsorbents having potential in ultrasound-assisted adsorptive removal of methylene blue dye from wastewater and antimicrobial activity, Materials 15 (2022) 1637.
[33] N.S.M. Saidi, H.M. Yusoff, I.U.H. Bhat, S. Appalasamy, A.D.M. Hassim, F. Yusoff, A. Asari, N.H.A. Wahab, Stability and antibacterial properties of green synthesis silver nanoparticles using Nephelium lappaceum peel extract, Malays. J. Anal. Sci. 24 (2020) 940–953.
[34] A. Kanchana, S. Devarajan, S.R. Ayyappan, Green synthesis and characterization of palladium nanoparticles and its conjugates from Solanum trilobatum leaf extract, NanoMicro Lett. 2 (2010) 169–176.
[35] M. Zare-Bidaki, A. Ghasempour, P. Mohammadparast-Tabas, S.M. Ghoreishi, E. Alamzadeh, R. Javanshir, B.N. Le, M. Barakchi, M. Fattahi, S. Mortazavi-Derazkola, Enhanced in vivo wound healing efficacy and excellent antibacterial, antifungal, antioxidant and anticancer activities via AgNPs@PCS, Arab. J. Chem. 16 (2023) 105194.
[36] G. Yildirim, A.B. Semerci, S. Saribulak, Green synthesis of silver nanoparticles (PA-AgNPs), characterisation, antibacterial and proliferative effects, Res. Pract. VETERINARY Anim. Sci. 2 (2025) 98–112.
[37] M. Asif, R. Yasmin, R. Asif, A. Ambreen, M. Mustafa, S. Umbreen, Green synthesis of silver nanoparticles (AgNPs), structural characterization, and their antibacterial potential, DoseResponse 20 (2022), 15593258221088709.
[38] H. Rizwana, N.A. Bokahri, F.S. Alkhattaf, G. Albasher, H.A. Aldehaish, Antifungal, antibacterial, and cytotoxic activities of silver nanoparticles synthesized from aqueous extracts of mace-arils of Myristica fragrans, Molecules 26 (2021) 7709.
[39] B. Das, S.K. Dash, D. Mandal, T. Ghosh, S. Chattopadhyay, S. Tripathy, S. Das, S. K. Dey, D. Das, S. Roy, Green synthesized silver nanoparticles destroy multidrug resistant bacteria via reactive oxygen species mediated membrane damage, Arab. J. Chem. 10 (2017) 862–876.
[40] F. Mariani, E.M. Galvan, Staphylococcus aureus in polymicrobial skinand soft tissue infections: impact of inter-species interactionsin disease outcome, Antibiotics 12 (2023) 1164.
[41] K. Jomova, S.Y. Alomar, S.H. Alwasel, E. Nepovimova, K. Kuca, M. Valko, Several lines of antioxidant defense against oxidative stress: antioxidant enzymes, nanomaterials with multiple enzyme-mimicking activities, and low-molecular-weight antioxidants, Arch. Toxicol. 98 (2024) 1323–1367.
[42] M.F. Baran, C. Keskin, A. Baran, A. Hatipoğlu, M. Yildiztekin, S. Küçükaydin, K. Kurt, H. Hoşgören, M.M.R. Sarker, A. Sufianov, O. Beylerli, R. Khalilov, A. Eftekhari, Green Synthesis of Silver Nanoparticles from Allium cepa L. Peel Extract, Their Antioxidant, Antipathogenic, and Anticholinesterase Activity, Molecules 28 (2023) 2310.
[43] I.M. Comino-Sanz, M.D. López-Franco, B. Castro, P.L. Pancorbo-Hidalgo, The role of antioxidants on wound healing: a review of the current evidence, J. Clin. Med. 10 (2021) 3558.
[44] F. Miere, A.C. Teuşdea, V. Laslo, S. Cavalu, L. Fritea, L. Dobjanschi, M. Zdrinca, M. Zdrinca, M. Ganea, P. Paşc, A.R. Memete, A. Antonescu, A.M. Vlad, S.I. Vicas, Evaluation of in vitro wound-healing potential, antioxidant capacity, and antimicrobial activity of Stellaria media (L.) Vill, Appl. Sci. 11 (2021) 11526.
[45] S.J. Jang, I.J. Yang, C.O. Tettey, K.M. Kim, H.M. Shin, In-vitro anticancer activity of green synthesized silver nanoparticles on MCF-7 human breast cancer cells, Materials Science Engineering C 68 (2016) 430–435.
[46] E.S. Al-Sheddi, N. Alsohaibani, N. bin Rshoud, M.M. Al-Oqail, S.M. Al-Massarani, N.N. Farshori, T. Malik, A.A. Al-Khedhairy, M.A. Siddiqui, Anticancer efficacy of green synthesized silver nanoparticles from Artemisia monosperma against human breast cancer cells, South Afr. J. Bot. 160 (2023) 123–131.
[47] M. Hashemabadi, H. Sasan, M. Amandadi, R. Mohammadinejad, G. Farnoosh, M. Azimzadeh, R.A. Taheri, Natural gum as bio-reductant to green synthesize silver nanoparticles: assessing the apoptotic efficacy on MCF-7 and SH-SY5Y cell lines and their antimicrobial potential, Polym. Bull. 78 (2021) 2867–2886.
[48] M. Oves, M. Ahmar Rauf, M. Aslam, H.A. Qari, H. Sonbol, I. Ahmad, G. Sarwar Zaman, M. Saeed, Green synthesis of silver nanoparticles by Conocarpus Lancifolius plant extract and their antimicrobial and anticancer activities, Saudi J. Biol. Sci. 29 (2022) 460–471.
[49] A.P. Ajaykumar, A. Mathew, A.P. Chandni, S.R. Varma, K.N. Jayaraj, O. Sabira, V. A. Rasheed, V.S. Binitha, T.R. Swaminathan, V.S. Basheer, S. Giri, S. Chatterjee, Green synthesis of silver nanoparticles using the leaf extract of the medicinal Plant, Uvaria narum and Its Antibacterial, Antiangiogenic, Anticancer and Catalytic Properties, Antibiotics 12 (2023) 564.
[50] K.D. Datkhile, S.R. Patil, P.P. Durgawale, M.N. Patil, N.J. Jagdale, V.N. Deshmukh, A.L. More, Biogenic silver nanoparticles synthesized using mexican poppy plant inhibits cell growth in cancer cells through activation of intrinsic apoptosis pathway, Nano Biomed. Eng. 12 (2020) 241–252.
[51] M.S. Khan, A. Alomari, S. Tabrez, I. Hassan, R. Wahab, S.A. Bhat, N.O. Alafaleq, N. Altwaijry, G.M. Shaik, S.K. Zaidi, W. Nouh, M.S. Alokail, M.A. Ismael, Anticancer potential of biogenic silver nanoparticles: a mechanistic study, Pharmaceutics 13 (2021) 707.
[52] Y.G. El-Baz, A. Moustafa, M.A. Ali, G.E. El-Desoky, S.M. Wabaidur, M.M. Faisal, An analysis of the toxicity, antioxidant, and anti-cancer activity of cinnamon silver nanoparticles in comparison with extracts and fractions of cinnamomum cassia at normal and cancer cell levels, Nanomaterials 13 (2023) 945.
[53] N.S. Alharbi, N.S. Alsubhi, Green synthesis and anticancer activity of silver nanoparticles prepared using fruit extract of Azadirachta indica, J. Radiat. Res. Appl. Sci. 15 (2022) 335–345.
[54] Z.A. Ratan, M.F. Haidere, M. Nurunnabi, S.M. Shahriar, A.J.S. Ahammad, Y. Y. Shim, M.J.T. Reaney, J.Y. Cho, Green chemistry synthesis of silver nanoparticles and their potential anticancer effects, Cancers 12 (2020) 855.
[55] M. Akter, M.T. Sikder, M.M. Rahman, A.K.M.A. Ullah, K.F.B. Hossain, S. Banik, T. Hosokawa, T. Saito, M. Kurasaki, A systematic review on silver nanoparticles-induced cytotoxicity: physicochemical properties and perspectives, J. Adv. Res. 9 (2018) 1–16.
[56] M. Rybka, Ł. Mazurek, M. Konop, Beneficial effect of wound dressings containing silver and silver nanoparticles in wound healing—from experimental studies to clinical practice, Life 13 (2023) 69.
[57] R. Meenalotchani, S. Nirenjen, M. Manisha, B.G. Prajapati, E. Arun, N. Afreen, S. S. Ankul, S. Sridevi, N. Harikrishnan, O.A. Alsaidan, Recent advances in silver nanoparticles for enhanced wound healing with mechanisms, formulations, and clinical insights, J. Drug Deliv. Sci. Technol. 114 (2025) 107437.

[58] K.M. Mukhtarovna, H.F. Shamikh Al-Saedi, O.M. Hameed, M. Jassim Al-saray, H. Hameed Jasim, F. Alajeeli, B. Ali Ahmed, A.K. Wabdan, Y. Ainur Shamakhankyzy, A. Khurramov, A. Umirzokov, B. Gulnaz, Histological and immunohistochemical evaluation of silver nanoparticle-mediated wound healing in rabbits, J. Nanostruct. 13 (2023) 747–754.

[59] S.N. Nandhini, N. Sisubalan, A. Vijayan, C. Karthikeyan, M. Gnanaraj, D.A. M. Gideon, T. Jebastin, K. Varaprasad, R. Sadiku, Recent advances in green synthesized nanoparticles for bactericidal and wound healing applications, Heliyon 9 (2023) e13128.

[60] N. Abbasi, H. Ghaneialvar, R. Moradi, M.M. Zangeneh, A. Zangeneh, Formulation and characterization of a novel cutaneous wound healing ointment by silver nanoparticles containing Citrus lemon leaf: a chemobiological study, Arab. J. Chem. 14 (2021) 103246.

[61] V. Lakkim, M.C. Reddy, V.V.V. Lekkala, V.R. Lebaka, M. Korivi, D. Lomada, Antioxidant efficacy of green-synthesized silver nanoparticles promotes wound healing in mice, Pharmaceutics 15 (2023) 1517.